Temporal and Spatial Behavior of Electron Density and Temperature in a Laser-Produced Plasma from $YBa_2Cu_3O_7$

S. S. HARILAL, C. V. BINDHU, V. P. N. NAMPOORI, and C. P. G. VALLABHAN*

Laser Division, International School of Photonics, Cochin University of Science and Technology, Cochin 682 022, India (S.S.H., C.V.B., V.P.N.N., C.P.G.V.); and Department of Physics, Sree Narayana College, Punalur 691 305, India (S.S.H.)

Spectroscopic studies of laser-induced plasma from a high-temperature superconducting material, viz., $YBa_2Cu_3O_7$ (YBCO), have been carried out. Electron temperature and electron density measurements were made from spectral data. The Stark broadening of emission lines was used to determine the electron density, and the ratio of line intensities was exploited for the determination of electron temperature. An initial electron temperature of 2.35 eV and electron density of 2.5×10^{17} cm^{-3} were observed. The dependence on electron temperature and density on different experimental parameters such as distance from the target, delay time after the initiation of the plasma, and laser irradiance is also discussed in detail.

Index Headings: **Laser-plasma spectroscopy; Plasma diagnostics; Emission spectroscopy; $YBa_2Cu_3O_7$.**

INTRODUCTION

Laser deposition of high-temperature superconducting (HTSC) material such as $YBa_2Cu_3O_7$ (YBCO) for thin-film preparation has recently attracted considerable attention from different groups of researchers.[1–3] Among the various methods for producing HTSC films, the laser deposition technique has gained wide acceptance. The technique is advantageous because of its highly directed and local nature and is capable of giving flexible control over the process parameters and the film composition, structure, and properties.[4] Laser radiation is being successfully used not only to deposit thin films onto the specially prepared substrates but also to effect some structural modifications of the deposited layer and to analyze the molecular composition and velocity distribution of particles encountering the substrate.[5,6] Among the parameters involved in the pulsed laser deposition process, the laser irradiance, laser wavelength, background gas pressure, and distance at which the substrate is placed seem to be more relevant in order to control the film growth. Spectral analysis of light emitted from the plasma produced in the process of target ablation and material transport in laser deposition of thin films gives information about the plasma composition, the energy content of ablation products, and the dynamics of the different species in the plume. In addition, the evolution of the plume can be theoretically predicted with models that refer to the initiation mechanism, kinetic processes, and other important parameters such as electron temperature and electron density, etc.

Laser ablation of HTSC targets is accompanied by the formation of brilliant elongated plasma located over the target surface, extending outwards. The length of the laser-ablated plasma plume depends on the laser irradiance employed as well as on the nature and pressure of the ambient gas used.[7–9] It was also noted that the expansion dynamics of various species in the plasma strongly depend on the laser irradiance used and distance z from the target surface.[10,11] Research on the ablation products of YBCO superconductors shows that there exist four types of particles: neutral atoms and oxide molecules, ions and ionized molecules, micro-clusters, and macro-particles.[12–16] Analysis of the optical emission spectrum from the plasma plume has been used to identify vaporized and ejected atoms, ionized atoms, and diatomic molecules, while mass spectroscopic studies can be successfully used for the study of micro-clusters and macro-particles. Identification of these species is important in understanding the complicated ablation, transport, and deposition processes.

An analysis of optical emission produced by laser ablation of a YBCO target with the use of a wide range of wavelengths showed that UV radiation (excimer lasers) produces mostly neutral species and that 1.06 μm and 532 nm radiation (Nd:YAG laser) produce mostly ionized species.[17,18] An excimer laser with high photon energy may cause internal electronic excitation. Also, YBCO has a smaller absorption coefficient for the longer wavelength in comparison to the UV region. More thermal effects can therefore be expected in the former case. An important difference between the excimer and YAG lasers is the much greater coherence of the YAG output, leading to vastly different far-field characteristics of the light source. Consequently, YAG laser excitation of the target occurs in a far more localized manner. Richter[19] demonstrated the peculiarities of the pulsed laser plasma method for the deposition of thin films by estimating the evaporation threshold as well as the electron temperature and density of the absorbing laser plasma.

Most of the published works have concentrated mainly on identification of plasma species and on parametric studies of the velocity distributions of species in the expanding plume.[20–23] However, relatively little quantitative information is available on either the fundamental plasma parameters, such as electron temperature, electron density, composition, etc., or on the nature of the dominant plume excitation processes in different spatial and temporal regions of the expanding plasma. Such data are required in order to develop and test models of plasma processes[24,25] that enable us to evaluate the energy transport into the plasma with regard to temporal and local behavior as well as its effectiveness in thin-film deposition.

There are several diagnostic techniques employed for the determination of electron density, which include plas-

Received 2 June 1997; accepted 18 September 1997.

* Author to whom correspondence should be sent.

0003-7028/98/5203-0449$2.00/0

ma spectroscopy,[26,27] Langmuir probe,[28,29] microwave and laser interferometry,[30–32] and Thomson scattering.[33,34] Thomson scattering is probably the most direct and least theory-dependent approach, while spectroscopy is the simplest as far as instrumentation is concerned. Plasma density determination using Stark broadening of spectral lines is a well-established and reliable technique[26,35,36] in the range of number density from 10^{14} to 10^{18} cm^{-3}. The electron temperature is an equally important plasma parameter, which can be determined spectroscopically in a variety of ways—from the ratio of the integrated line intensities, from the ratio of the line intensity to underlying continuum, and from the shape of the continuum spectrum (*bremsstrahlung*).[37]

In the present paper, we report the studies on plasma parameters such as electron density and electron temperature and their dependence on factors such as incident laser irradiance, time after the elapse of the laser pulse, and spatial separation from the target surface. The relative spectral line intensities of successive ionization states of barium were used for the determination of electron temperature, while the Stark broadened profile of Ba(I) at the 553.5 nm transition is used for the measurement of electron density.

EXPERIMENTAL

Details of the experimental technique are given elsewhere.[38,39] The plasma was generated by ablation of a high-temperature superconducting YBCO sample using 1.06 μm radiation pulses from a Q-switched Nd:YAG laser (Quanta Ray, DCR II) with a repetition rate of 10 Hz and pulse width of 9 ns (maximum energy 275 mJ). The estimated spot size at the target was 200 μm. The target in the form of a disk-shaped pellet (25 mm diameter and 5 mm thickness) was placed in an evacuated chamber provided with optical windows for laser irradiation and spectroscopic observation of the plasma produced from the target. During these studies the pressure inside the vacuum chamber was maintained at $\sim 10^{-4}$ mbar. The target was rotated about an axis parallel to the laser beam to avoid nonuniform pitting of the target surface. The bright plasma emission was viewed through a side window at right angles to the plasma expansion direction. The section of the plasma was imaged onto the slit of a 1 m Spex monochromator (Model 1704, grating with 1200 grooves per mm blazed at 500 nm, maximum resolution 0.015 nm), with entrance and exit slits kept parallel to the target surface, and the use of appropriate collimating and focusing lenses in order to have one-to-one correspondence of the sampled area of the plasma with the image. The spatial resolution available was better than 0.2 mm. The recording was done by using a thermoelectrically cooled Thorn EMI photomultiplier tube, which was coupled to a boxcar averager/gated integrator (Standford Research Systems, SRS 250). The averaged output from the boxcar averager was fed to a chart recorder, which for the present study averaged out intensities from 10 pulses. For the calculation of electron temperature, emission intensities were corrected for the detector spectral response, which was predetermined through use of a standard lamp.

RESULTS AND DISCUSSION

One of the most powerful spectroscopic techniques to determine the electron density with reasonable accuracy is by the measurements of a Stark-broadened line profile of an isolated atom or singly charged ion.[26,27] For the estimation of electron density, the Stark-broadened profile of the Ba(I) transition ($6p^1\ P_1^2$–$6s^1\ S_0$) at 553.5 nm was charted, with the monochromator kept at its maximum resolution. Three broadening mechanisms are likely to contribute significantly to linewidths observed in plasmas produced during pulsed laser ablation, viz., Doppler broadening, resonance pressure broadening, and Stark broadening. Doppler broadening arises because of different Doppler shifts (i.e., $\Delta\lambda = \lambda\upsilon_z/c$) experienced by the ablated species in different regions of the plume having different velocity components υ_z in the direction of observation. Since the expansion velocities[40] of Ba(I) are found to be $\sim 5 \times 10^5$ cm s^{-1}, which corresponds to Doppler linewidths [full width at half-maximum (FWHM)] ~ 0.1 A^0, the effect due to Doppler broadening can be ignored here. The pressure broadening is proportional to the ground-state number density of the corresponding species and transition oscillator strength. The reported value for resonance broadening for Ba(I) at 553.5 nm is relatively small,[41] and hence the contribution due to this type of broadening can be neglected. Under these conditions Stark broadening is the dominant broadening process. Stark broadening of spectral lines in plasmas results from collisions with charged species resulting in both broadening of the line and shift in the peak wavelength.

The full width at half maximum of the Stark-broadened lines $\Delta\lambda_{1/2}$ is related to the electron density by the expression[26]

$$\Delta\lambda_{1/2} = 2W\left[\frac{n_e}{10^{16}}\right] + 3.5A\left[\frac{n_e}{10^{16}}\right]^{1/4}\left[1 - \frac{3}{4}N_D^{-1/3}\right]W\left[\frac{n_e}{10^{16}}\right]A^0 \quad (1)$$

where W is the electron impact parameter, which can be incorporated with different temperatures; A, the ion broadening parameter; and N_D, the number of particles in the Debye sphere. The first term on the right side of Eq. 1 represents the broadening due to the electron contribution, and the second term is the ion correction factor. For nonhydrogenic ions, Stark broadening is predominantly caused by electron impact. Since the perturbations caused by ions are negligible compared with those from electrons, the ion correction factor can safely be neglected. Therefore Eq. 1 reduces to

$$\Delta\lambda_{1/2} = 2W\left[\frac{n_e}{10^{16}}\right]A^0. \quad (2)$$

The electron impact parameter (W) values for the Ba(I) 553.5 nm transition are not available in the literature, but values are available for the corresponding $nsnp^1\ P_1^0 \rightarrow ns^{21}\ S_0$ transitions of the elements Mg, Be, and Ca from the same periodic group.[42] The latter values increase approximately linearly with n^2, and this dependence was extrapolated to yield a W value of $\sim 1.6 \times 10^{-2}$ A^0 for the Ba(I) 553.5 nm transition at a temperature of 10 000

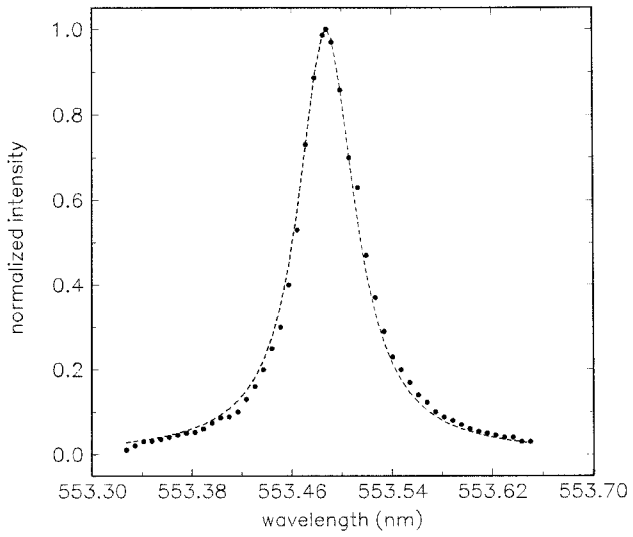

FIG. 1. Typical Stark-broadened profile of the Ba(I) transition at 553.5 nm. The FWHM of this line is used to infer electron density. The dotted line in the figure represents a fitted Lorentzian curve.

K. Since W values are weak functions of temperature and vary by a factor less than 2 over the temperature range 10 000 K–80 000 K, the determination of electron density deduced with the use of this W value can be considered as reliable. We have measured electron density using the Stark broadening method as functions of separation from the target, time after the elapse of laser pulse, and laser irradiance. A typical Stark-broadened profile of Ba(I) at the 553.5 nm line with a theoretically fitted Lorentzian curve is given in Fig. 1.

Relative line intensities from the same element and ionization state usually do not provide accurate temperatures. The principal reason for this limitation is the relatively small separation between the upper levels of two lines. Considerable improvement in sensitivity can be obtained by selecting lines from successive ionization states of the same element, because the effective energy difference is now enhanced by the ionization energy, which is much larger than the thermal energy. In local thermodynamic equilibrium (LTE), the ratio of such line intensities is given by[26]

$$\frac{I'}{I} = \left[\frac{f'g'\lambda^3}{fg\lambda'^3}\right][4\pi^{3/2}a_0{}^3n_e]^{-1}\left[\frac{kT_e}{E_H}\right]^{3/2}\exp\left[\frac{-(E'+E_\infty-E-\Delta E_\infty)}{kT}\right] \quad (3)$$

where the primed symbols represent the line of the atom with higher ionization state and where f is the oscillator strength; g, the statistical weight; a_0, the Bohr radius; E_H, the ionization energy of the hydrogen atom; E, the excitation energy; and ΔE_∞, the correction to the ionization energy E_∞ of the lower ionization stage due to plasma interactions.

The correction factor in the ionization energy is given by

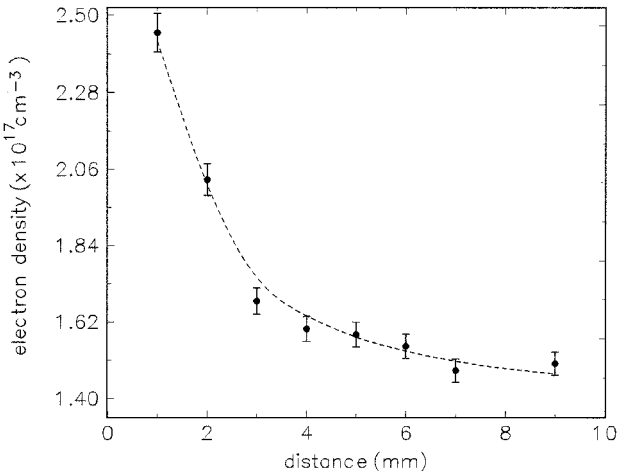

FIG. 2. Electron density as a function of distance. Laser irradiance, 42 GW cm^{-2}. The dotted line in the figure represents the fitted $1/z$ curve.

$$\Delta E_\infty = 3z\frac{e^2}{4\pi\epsilon_0}\left[\frac{4\pi n_e}{3}\right]^{1/3} \quad (4)$$

where $z = 2$ for the lower ionization state.[26]

For temperature calculations, we made use of recorded intensities for the Ba(II) 614 and 649.8 nm lines and Ba(I) 577.7 and 553.5 nm lines. Details of the spectroscopic constants of these lines were taken from Griem.[26]

Spatial Dependence. When the laser is focused onto the YBCO, which is placed in vacuum, a rapid expansion takes place because of density gradients in the plasma. Figures 2 and 3 represent plots of electron density and temperature, respectively, as a function of distance. The Stark-broadened profile of the Ba(I) transition at 553.5 nm was used for density calculations, while line intensities of successive ionization stages were used for the electron temperature measurements. All the results were obtained in a direction of the expanding plasma plume axis at different distances from the target surface and at a laser irradiance of 42 GW cm^{-2}. The estimation of n_e and T_e of the laser-produced YBCO plume was carried out for distances up to 12 mm from the target surface in

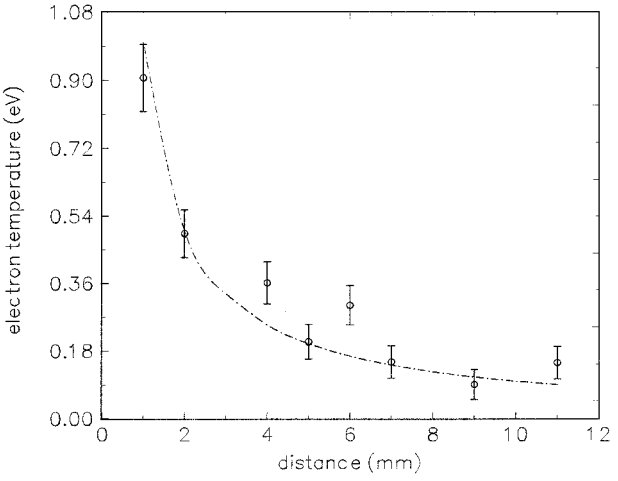

FIG. 3. The variation of electron temperature with distance from the target surface at a laser irradiance of 42 GW cm^{-2}. The dotted line in the figure represents the fitted $z^{-0.8}$ curve.

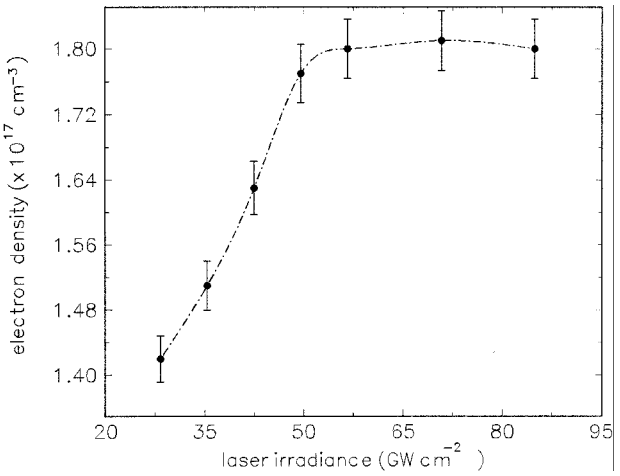

FIG. 4. Electron density as a function of laser irradiance. The spectra were sampled at a distance 3 mm from the target surface.

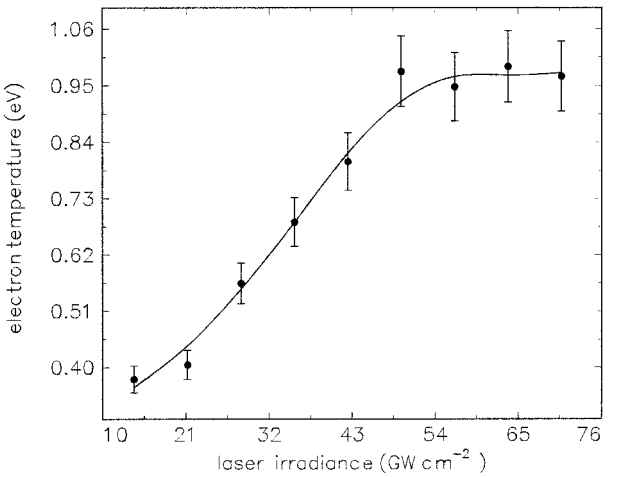

FIG. 5. Electron temperature as a function of laser irradiance (distance 3 mm).

a time-integrated manner. The electron density was found to decrease rapidly from 2.4×10^{17} cm^{-3} at 1 mm to 1.55×10^{17} cm^{-3} at 3 mm and to level off at higher distances.

The density gradients of the plasma at a point z and at a time t can be expressed as[1,43]

$$n_e(z, t) = n_0(t)\left[1 - \frac{z}{Z(t)}\right] \quad (5)$$

where n_0 is the density at the center of the laser-irradiated spot ($z = 0$) at time t; z is the coordinate perpendicular to the target; and $Z(t)$ refers to the spatial coordinate of the leading edge of the plasma. According to Eq. 5, the electron density should be decreased linearly with distance from the target surface. However, in actual practice the density gradient does not decrease linearly. The decrease of electron density as a function of distance shows a z^{-1} dependence. The electron density in the plasma core decreases with distance because of the expansion of the plasma and also because of recombination and diffusion within the plasma volume. The much faster decrease near the target surface may be caused by plasma cooling due to condensation and recombination. The variation of n_e as a function of distance follows approximately a $1/z$ law at short distances, indicating that the initial expansion of the electron gas is one-dimensional, in good agreement with the predictions of the plume expansion model given by Singh and Narayan.[1]

The electron temperature close to the target is about 1.2 eV and it decreases with increasing separation from the target surface; at 5 mm distance, the electron temperature drops to 0.18 eV. At distances greater than 5 mm from the target surface, the electron temperature is almost constant. At distances close to the target, the thermal energy is rapidly converted into the kinetic energy, with plasma attaining maximum expansion velocities and thereby causing the temperature to drop off rapidly as the plasma expands. But at greater distances, the temperature drop is smaller and a saturation is observed because of energy gained in the recombination of ions. The variation of electron temperature shows a $z^{-0.8}$ dependence with distance.

Effect of Laser Irradiance. The nature and characteristics of the laser-produced plasma strongly depend on the laser irradiance levels used. Figures 4 and 5 give the variation of electron density as a function of laser irradiance used for the ablation. The Stark-broadened spectra are recorded in a time-integrated manner in which the plasma plume is sampled at a distance 3 mm from the target surface. As laser irradiance increases from 28 GW cm^{-2} to 55 GW cm^{-2}, electron density varies rapidly from 1.42×10^{17} cm^{-3} to 1.8×10^{17} cm^{-3}, and then it remains more or less at a constant value. As the laser irradiance increases, the number of free electrons increases and consequently the electron density as well. With increase in laser irradiance, the electron temperature is also found to increase up to a threshold irradiance and then to saturate. The saturation in electron density and temperature at high irradiance levels is presumably due to plasma shielding, i.e., absorption and/or reflection of the laser photons by the plasma itself.[37] The reflection of the incident laser photon depends on the plasma frequency ν_p, which should be lower than the laser frequency. A Nd:YAG laser with its fundamental wavelength (1.06 μm) corresponds to a frequency $\nu_l = 2.828 \times 10^{14}$ Hz. The plasma frequency is given by $\nu_p = 8.9 \times 10^3 n_e^{0.5}$, where n_e is the electron density. Calculations show that, with $n_e \sim 10^{17}$ cm^{-3}, $\nu_p = 6.5 \times 10^{12}$ Hz, which is much smaller than the laser frequency. So the energy losses due to reflection of the Nd:YAG laser beam from the plasma can be assumed to be insignificant.

The absorbing plasma generated by the leading edge of the laser pulse prevents light from reaching the surface. Therefore, most of the energy in the remaining part of the laser pulse will be absorbed by material in front of the surface. The surface is effectively cut off from the trailing edge of the incoming laser pulse. Thus the given amount of energy delivered at high power is less effective in causing vaporization than the energy delivered at lower powers. The prominant mechanism responsible for plasma absorption at these laser irradiance levels used is inverse *bremsstrahlung*.[44] The saturation in T_e and n_e at higher irradiances cannot be explained by considering only the prominent absorption mechanisms via inverse *bremsstrahlung*. Such temperature and density behavior can be explained by assuming the formation of a self-

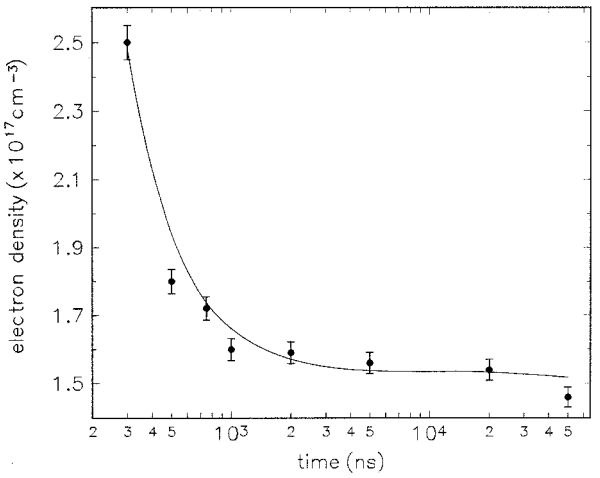

FIG. 6. Temporal evolution of electron density at a distance 3 mm from the target surface. Laser irradiance, 42 GW cm^{-2}.

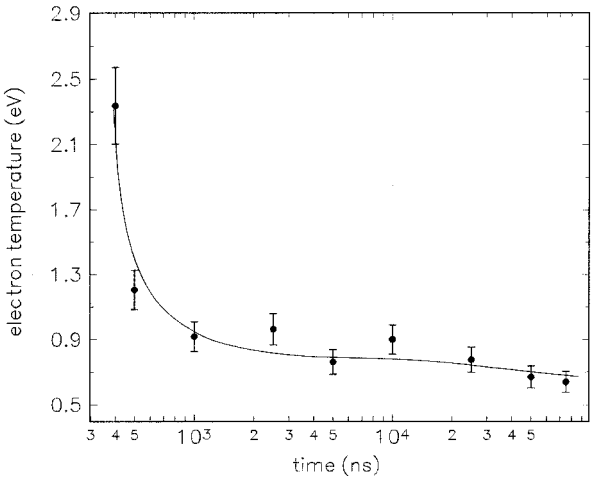

FIG. 7. The variation of electron temperature with time. These spectra were recorded at distance 3 mm and at a laser irradiance of 35 GW cm^{-2}.

regulating regime at higher irradiances.[43] At high irradiance levels, when an appreciable amount of energy is absorbed by the plasma, a self-regulating regime may form near the target surface. If the absorption of the laser photons by the plasma becomes higher because of high plasma density, the evaporation of the species from the target becomes less, which in turn decreases the density of the charged species. This behavior consequently increases the absorption of the laser photons by the target, which in turn increases the temperature of the plasma. On the other hand, when the absorption of the laser energy is less, the process is reversed, with similar results. It has been theoretically proved that[45] the density, temperature, and dimensions of the plume adjust in such a manner that the plasma absorbs the same amount of laser radiation to maintain a self-regulating regime. This assumption was found to be valid in laser-generated plasma, where thermalization time is significantly less than the plasma expansion time, resulting in an establishment of uniform temperature in the plasma. The thermalization time τ_{ei} of energy exchange between electron and ions during collision can be estimated from the relation[46]

$$\tau_{ei} = \frac{252\,MT_e^{3/2}}{\ln(\Lambda)n_e} \tag{6}$$

where

$$\Lambda = \frac{3(kT)^{3/2}}{4(\pi n_e)^{1/2}e^3} \tag{7}$$

and $\ln(\Lambda)$ stands for the Coulomb logarithm, which involves dynamical information about ion–electron collisions, and M is atomic weight. With $n_e = 10^{17}$ cm^{-3}, $T_e \approx T$ (vapor temperature) $= 1$ eV, the relaxation time is on the order of a few picoseconds, which is much smaller than the expansion time or pulse width of the laser beam, which is on the order of a few nanoseconds.

We have also observed a peak shift in the line center with increasing irradiance. The observed asymmetry of our time-integrated emission line shapes is consistent with what would be expected for a convolution of various Stark shifts towards the red, which will arise from differing electron densities within the plume volume sampled, caused by different irradiance levels.

Time Dependence. The variation of electron temperature and electron density with respect to spatial position and laser irradiance described in the previous sections was studied with the use of time-integrated emission spectroscopy. The calculated time-integrated electron temperature and density represent the average behavior of these parameters at different times. These measurements may be influenced by the expansion of the plasma relative to integration time.[47]

We studied temporal variation of electron temperature and density with an integration time of 10 ns. For an integration time of 10 ns, the spatial distance traversed by Ba ions is 0.07 mm, taking the average expansion velocity[47] as 7×10^5 cm s^{-1} at a laser irradiance of 42 GW cm^{-2}, which is much smaller than the successive spatial steps of 1 mm. Hence, there will not be any significant mixing of spatial and temporal aspects of the plasma, and an effective separation of spatial and temporal effects can be achieved. The temporal evolution of electron density deduced from Stark broadening of the Ba(I) 553.5 nm transition is shown in Fig. 6 (distance 3 mm, laser irradiance 42 GW cm^{-2}). Since the spectral line emission front is masked by the continuum emission, the electron density for time < 200 ns could not be measured by this method. The continuum stems from the elastic collision of electrons with ions and black-body emission by plasma. The intensity of the continuum decreases with increasing delay time. Nevertheless, we can characterize the temporal evolution of n_e, which is found to diminish rapidly with time up to 500 ns and then to level off. The fast decay rate can be attributed to the plasma propagation, while the slowing and leveling off at longer times are probably due to recombination. It may also be noted that electron density shows a t^{-2} dependence on time. The calculated plasma temperature and its variation as a function of time after the initiation of the plasma are shown in Fig. 7. In the early stage of plasma evolution, the electron temperature is very high and is changing very rapidly. However, at greater duration times (>1 μs), the plasma is found to be cooled to much lower temperatures, and thereafter temperature continues to remain very stable, around 0.6–0.7 eV for a long period.

The electron temperature follows a t^{-2} dependence on time during the initial periods up to ~ 1 μs, which is in accordance with the theoritical adiabatic model by Rumbsy and Paul.[48]

Local Thermodynamic Equilibrium. For our analysis of electron temperature, we have assumed that the plasma is in local thermodynamic equilibrium. In a transient system such as the plasma formed by a pulsed laser beam, for LTE to hold good, the electron–atom and electron–ion collision processes must be extremely rapid and must dominate the radiative processes. In a system that is at LTE, particles will have Maxwellian velocity distributions, populations in the energy levels will follow Boltzmann statistics, ionization processes will be described by Saha's equation, and radiation density will obey Planck's law. Along the boundary of the plasma, where the number densities are low and movement of the boundary region is rapid, LTE is probably not a good assumption. However, slightly deeper into the plasma volume, where conditions change more slowly and collisions occur more frequently, this assumption is valid. In our experiment the apparent length of the plasma is ~ 3 cm, and studies were made for distances up to 11 mm from the target. Similar conditions are also valid in the case of time elapsed after the laser pulse (i.e., for time intervals on the order of few microseconds). Clearly for LTE to hold, the electron density must be sufficiently high. It is worthwhile to check the minimum density condition for LTE,[49] viz.,

$$n_e \geq 1.4 \times 10^{14}\ T_e^{1/2}\ (\Delta E)^3\ \text{cm}^{-3}. \qquad (8)$$

For the transition with the largest gap (553.5 nm), ΔE = 2.24 eV and at the highest temperature, 2.5 eV, the lower limit for n_e is 2.5×10^{15} cm^{-3}. Our observed values of n_e are always greater than this limit, implying that the LTE approximation assumed for our analysis is valid.

CONCLUSION

The $YBa_2Cu_3O_7$ target is laser ablated, and the estimations of electron temperature and electron density of the resultant plasma plume have been carried out by spectroscopic means. The line intensities of the successive ionization states were used for the determination of the electron temperature, and the Stark-broadened profile of the Ba(I) transition at 553.5 nm was used for the measurement of electron density.

Measurements of the line intensities of electronically excited Ba atoms and Ba ions were used to infer electron temperature at several positions located away from the target surface and its variation as a function of time elapsed after the initiation of plasma. The electron temperature has $z^{-0.8}$ and t^{-2} dependence on distance and time, respectively. The variation of electron temperature with laser irradiance shows a saturation at high irradiance levels, and this observation can be explained by assuming the formation of a self-regulating regime.

The Stark-broadened profile was exploited for the determination of electron density and its variation with distance from the target surface, time after the initiation of plasma, and laser irradiance. The electron density variation shows z^{-1} dependence on distance from the target surface, while a t^{-2} type variation is found to hold good with respect to the time elapsed after the laser pulse. At higher irradiance levels, a saturation effect on electron density was also observed due to plasma shielding.

ACKNOWLEDGMENTS

The present work is partially supported by the Department of Science and Technology, Government of India. S.S.H. and C.V.B. are grateful to the Council of Scientific and Industrial Research, New Delhi and the University Grant Commission, New Delhi for their fellowships.

1. R. K. Singh and J. Narayan, Phys. Rev. B **41,** 8843 (1990).
2. *Pulsed Laser Deposition of Thin Films*, D. B. Chrisey and G. K. Hubler, Eds. (Wiley, New York, 1994).
3. E. N. Sobol, *Phase Transformations and Ablation in Laser Treated Solids* (John Wiley and Sons, New York, 1995).
4. D. B. Geohegan, Thin Solid Films **220,** 138 (1992).
5. S. S. Harilal, P. Radhakrishnan, V. P. N. Nampoori, and C. P. G. Vallabhan, Appl. Phys. Lett. **64,** 3377 (1994).
6. Y. Nakata, W. K. A. Kumuduni, T. Okada, and M. Maeda, Appl. Phys. Lett. **64,** 2599 (1994).
7. A. Mele, A. G. Guidoni, R. Kelly, A. Miotello, S. Orlando, and R. Teghill, Appl. Sur. Sci. **96–98,** 102 (1996).
8. S. I. Anisimov, B. S. Lukyanchuk, and A. Luches, Appl. Sur. Sci. **96–98,** 96 (1996).
9. S. S. Harilal, R. C. Isaac, C. V. Bindhu, V. P. N. Nampoori, and C. P. G. Vallabhan, Jpn. J. Appl. Phys. **36,** 134 (1997).
10. S. S. Harilal, R. C. Issac, C. V. Bindhu, V. P. N. Nampoori, and C. P. G. Vallabhan, J. Appl. Phys. **80,** 3561 (1996).
11. S. S. Harilal, R. C. Issac, C. V. Bindhu, V. P. N. Nampoori, and C. P. G. Vallabhan, J. Appl. Phys. **81,** 3637 (1997).
12. G. Padmaja, A. V. Ravikumar, V. P. N. Nampoori, and C. P. G. Vallabhan, Bull. Mat. Sci. **14,** 545 (1991).
13. H. Chiba, K. Murakami, O. Eryu, K. Shihoyama, and K. Masuda, Jpn. J. Appl. Phys. **30,** L732 (1991).
14. O. Eryu, K. Murakami, K. Masuda, K. Shihoyama, and T. Mochizuki, Jpn. J. Appl. Phys. **31,** L86 (1992).
15. T. Venkateshan, X. D. Wu, A. Inam, Y. Jeon, M. Croft, E. W. Chase, C. C. Chang, and J. Wachtman, Appl. Phys. Lett. **53,** 1431 (1988).
16. A. V. Bulgakov, M. R. Predtechensky, and A. P. Mayorov, Appl. Sur. Sci. **96–98,** 159 (1996).
17. L. Lynds, B. R. Weinberger, B. M. Potrepka, G. G. Peterson, and M. P. Lindsay, Physica C **159,** 61 (1989).
18. H. S. Kwok, P. Mattocks, L. Shi, X. W. Wang, S. Witanachchi, Q. Y. Ying, J. P. Zheng, and D. T. Shaw, Appl. Phys. Lett. **52,** 1825 (I1988).
19. A. Richter, Thin Solid Films **188,** 275 (1990).
20. D. B. Geohegan, Appl. Phys. Lett. **60,** 2732 (1992).
21. W. K. A. Kumudini, Y. Nakata, T. Okada, and M. Maeda, Appl. Phys. B. **58,** 289 (1994).
22. J. Gonzalo, C. N. Afonso, and J. Perrière, J. Appl. Phys. **79,** 8042 (1996).
23. W. A. Weimer, Appl. Phys. Lett. **52,** 2171 (1988).
24. H. C. Le, J. Vuillon, D. Zeitoun, W. Marine, M. Sentis, and R. W. Dreyfus, Appl. Sur. Sci. **96–98,** 76 (1996).
25. V. I. Mazhukin, I. Smurov, and G. Flamant, Appl. Sur. Sci. **96–98,** 89 (1996).
26. H. R. Griem, *Spectral Line Broadening by Plasmas* (Academic Press, New York, 1974).
27. H. R. Griem, *Plasma Spectroscopy* (McGraw-Hill, New York, 1964).
28. J. N. Leboeuf, K. R. Chen, J. M. Donato, D. B. Geohegan, C. L. Liu, A. A. Puretzky, and R. F. Wood, Appl. Sur. Sci. **96–98,** 14 (1996).
29. D. B. Geohegan and A. A. Puretzky, Appl. Sur. Sci. **96–98,** 131 (1996).
30. M. A. Heald and C. B. Wharton, *Plasma Diagnostics with Microwaves* (Wiley, New York, 1965).
31. G. K. Varier, R. C. Isaac, C. V. Bindhu, S. S. Harilal, V. P. N. Nampoori, and C. P. G. Vallabhan, Spectrochim. Acta B **52,** 657 (1997).
32. T. Mochizuki, K. Hirata, H. Ninomiya, K. Nakamura, K. Maeda, S. Horiguchi, and Y. Fujiwara, Opt. Commn. **72,** 302 (1989).
33. M. C. M. Van de Sanden, J. M. de Regt, G. M. Janssen, J. A. M.

Van der Mullen, D. C. Schram, and B. Van der Sijde, Rev. Sci. Instrum. **63,** 3369 (1992).
34. S. B. Cameron, M. D. Tracy, and J. F. Camacho, IEEE Trans. Plas. Sci. **24,** 45 (1996).
35. C. C. Smith and N. J. Peacock, J. Phys. B **11,** 2749 (1978).
36. M. Galanti and N. J. Peacock, J. Phys. B **8,** 2427 (1975).
37. J. F. Ready, *Effect of High Power Laser Radiation* (Academic Press, New York, 1971).
38. S. S. Harilal, R. C. Isaac, C. V. Bindhu, V. P. N. Nampoori, and C. P. G. Vallabhan, Pramana **46,** 145 (1996).
39. S. S. Harilal, R. C. Isaac, C. V. Bindhu, P. Gopinath, V. P. N. Nampoori, and C. P. G. Vallabhan, Spectrochim. Acta A **53,** 1527 (1997).
40. S. S. Harilal, Ph.D. thesis, Cochin University of Science & Technology, Cochin, India (1997).
41. D. B. Geohegan, in *Pulsed Laser Deposition of Thin Films,* D. B. Chrisey and G. K. Hubler, Eds. (Wiley, New York, 1994).
42. A. H. El-Astal and T. Morrow, J. Appl. Phys. **80,** 1156 (1996).
43. R. K. Singh, O. W. Holland, and J. Narayan, J. Appl. Phys. **68,** 233 (1990).
44. S. S. Harilal, C. V. Bindhu, R. C. Isaac, V. P. N. Nampoori, and C. P. G. Vallabhan, J. Appl. Phys. **82,** 2140 (1997).
45. A. Caruso and R. Gratton, Plasma Phys. **10,** 867 (1968).
46. Y. B. Zeldovich and Y. P. Raizer, *Physics of Shock Waves and High-Temperature Hydrodynamic Phenomena* (Academic Press, New York, 1966).
47. X. L. Mao, M. A. Shannon, A. J. Fernandez, and R. E. Russo, Appl. Spectrosc. **49,** 1054 (1995).
48. P. T. Rumsby and J. W. M. Paul, Plasma Phys. **16,** 247 (1974).
49. G. Bekefi, *Principles of Laser Plasmas* (John Wiley and Sons, New York, 1976).